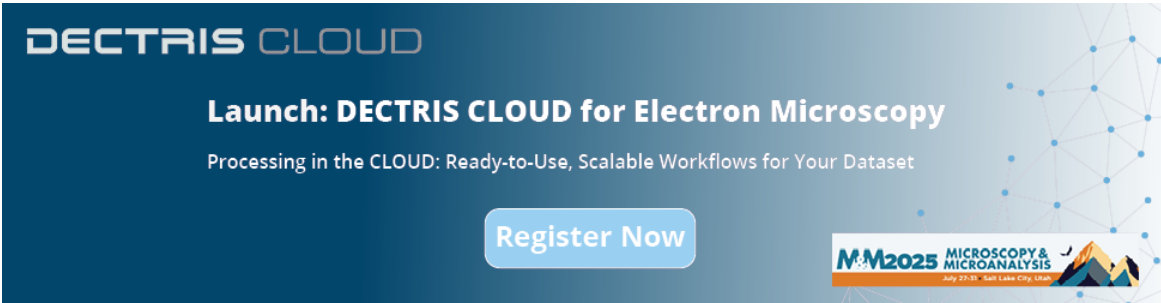


Smart Scanning Ion-Conductance Microscopy Imaging Technique Using Horizontal Fast Scanning Method

Jian Zhuang, Zhiwu Wang, Zeqing Li, Pengbo Liang, Mugubo Vincent



DECTRIS CLOUD

Launch: DECTRIS CLOUD for Electron Microscopy

Processing in the CLOUD: Ready-to-Use, Scalable Workflows for Your Dataset

[Register Now](#)

M2025 MICROSCOPY & MICROANALYSIS
July 27-31 • Salt Lake City, Utah

The banner features a dark blue background with a network of white dots and lines on the right side. The text is in white and light blue. A light blue button with the text 'Register Now' is positioned in the lower right. A logo for 'M2025 MICROSCOPY & MICROANALYSIS' is in the bottom right corner, including the dates 'July 27-31' and location 'Salt Lake City, Utah'.

Original Article

Smart Scanning Ion-Conductance Microscopy Imaging Technique Using Horizontal Fast Scanning Method

Jian Zhuang^{1,2}, Zhiwu Wang^{1,2}, Zeqing Li², Pengbo Liang^{1,2} and Mugubo Vincent^{1,2}

¹Key Laboratory of Education Ministry for Modern Design Rotor-Bearing System, Xi'an Jiaotong University, Xi'an 710049, China and ²School of Mechanical Engineering, Xi'an Jiaotong University, Xi'an 710049, China

Abstract

To solve extended acquisition time issues inherent in the conventional hopping-scanning mode of scanning ion-conductance microscopy (SICM), a new transverse-fast scanning mode (TFSM) is proposed. Because the transverse motion in SICM is not the detection direction and therefore presents no collision problem, it has the ability to move at high speed. In TFSM, the SICM probe gradually descends in the vertical/detection direction and rapidly scans in the transverse/nondetection direction. Further, the highest point that decides the hopping height of each scanning line can be quickly obtained. In conventional hopping mode, however, the hopping height is artificially set without *a priori* knowledge and is typically very large. Consequently, TFSM greatly improves the scanning speed of the SICM imaging system by effectively reducing the hopping height of each pixel. This study verifies the feasibility of this novel scanning method via theoretical analysis and experimental study, and compares the speed and quality of the scanning images obtained in the TFSM with that of the conventional hopping mode. The experimental results indicate that the TFSM method has a faster scanning speed than other SICM scanning methods while maintaining the quality of the images. Therefore, TFSM provides the possibility to quickly obtain high-resolution three-dimensional topographical images of extremely complex samples.

Key words: scanning ion-conductance microscopy (SICM), transverse-fast scanning mode (TFSM), living cells, imaging speed, imaging stability

(Received 22 June 2017; revised 24 March 2018; accepted 1 May 2018)

Introduction

Using a scanning probe microscope to achieve three-dimensional topographic imaging of living biological cells and dynamic observation has been a long-time challenge, but the advent of the scanning ion-conductance microscope (SICM) has provided an important development thereto. As a potential new member of the scanning probe microscope techniques, SICM was first proposed and invented by Hansma et al. in 1989. Because SICM uses the detected ion current flowing through the tip of its micropipette to control the distance between its probe and the sample surface, it can realize noncontact, high-resolution imaging for biological samples in a physiological environment (Korchev et al., 1997; Shevchuk et al., 2006). In recent years, SICM has been widely used in quantitative transmission of nanoparticles (Bruckbauer et al., 2002; Babakinejad et al., 2013; Ivanov et al., 2015), in drug reactions of biological micro-organizations (Yang et al., 2012) and in electrochemical detection (Takahashi et al., 2010; Nadappuram et al., 2013; O'Connell et al., 2014; Şen et al., 2015). It thus has widespread and promising applications in micro- and nanofabrication, materials research and development, stoichiological research and drug development.

Hansma et al. (1989) further proposed a direct current (DC) scanning mode, which maintains a constant ion current during the scanning process by controlling the *z*-direction motion of the micropipette. However, the ion current is inevitably affected by ionic current drift in the DC scanning process, resulting in collisions between the tip of the micropipette and the sample surface and thereby reducing the imaging stability.

To improve the SICM imaging stability and accuracy and its capability for imaging complex surface samples, various research groups have developed several important imaging modes. Pastre et al. (2001) and Shevchuk et al. (2001) have developed a distance modulation scanning mode, named the alternating current (AC) mode. In this mode, the SICM images using a probe that vibrates with an amplitude of a few dozen nanometers, where the amplitude of the AC ionic current is detected using a lock-in amplifier locked to the vibration frequency of the probe (Proksch et al., 1996; Pastre et al., 2001). This AC mode can overcome the effects of ionic current drift and improve the imaging stability and the sensitivity to distance measurements, but the vibration frequency of the probe restricts its scanning speed. McKelvey et al. (2014) and Li et al. (2014) have separately proposed another modulation scanning mode that applies an oscillating bias between a quasi-reference counter electrode (QRCE) in the probe and a second QRCE in the bulk solution to eliminate any physical oscillation of the probe, thereby generating an oscillating ion current feedback signal. Mann et al. (2002) have developed the

Author for correspondence: Jian Zhuang, E-mail: zhuangjian@mail.xjtu.edu.cn

Cite this article: Zhuang J, Wang Z, Li Z, Liang P, Vincent M (2018) Smart Scanning Ion-Conductance Microscopy Imaging Technique Using Horizontal Fast Scanning Method. *Microsc Microanal* 24(3): 264–276. doi: 10.1017/S1431927618000375

backstep mode and after implementing further refinements, Novak et al. (2009) have developed the hopping mode to further improve the SICM imaging stability for biological samples with complex topographies. The hopping mode greatly enhances the SICM imaging capability and stability, but it inevitably reduces the scanning speed of the probe. Zhukov et al. (2012) have proposed a hybrid scanning mode for fast SICM that quickly scans on samples with relatively flat surfaces and, to some extent, compensates for the hopping mode. Zhuang et al. (2017) have proposed a new scanning mode by utilizing the pipette predicted movement in the horizontal direction. In this method, the pipette parameters, such as the half cone angle, the ratio of the inner to outer radius, and the opening radii of the pipette tip, play a critical role in anticipating the upcoming raised topography in the horizontal direction. To achieve a maximal detectable distance, it is necessary to balance the relationships between the above-mentioned parameters. In addition, it is also necessary to balance the relationship between signal-to-noise ratios of the ionic current and the feedback threshold (Zhuang et al., 2017).

Hitherto, the majority of the existing SICM systems have adopted the conventional hopping mode, which takes a long time to image samples with complex topographies. This paper proposes a new scanning method to improve on the scanning speed of the traditional hopping mode without sacrificing its powerful detection capability. First, a home-built SICM system is developed that can operate in a new transverse-fast scanning mode (TFSM). Then, we report on contrast experiments carried out with TFSM on polydimethylsiloxane (PDMS) samples, human breast cancer cells and hippocampal neuronal cells with complex morphologies. Finally, the imaging speed and quality of SICM systems operating in the traditional hopping mode and in TFSM are compared with determine whether TFSM exhibits a better scanning speed without reducing the imaging quality.

Theoretical Analysis

Principles of the Method

The imaging speed of the conventional hopping mode of SICM is slow, mainly owing to the following two aspects: first, owing to the influence of the movement inertia, the probe continues to move in the original direction for a distance after reaching the target location. As the probe speed is increased, the influence of the movement inertia will also increase. Because the probe speed in the z -direction directly affects the SICM imaging quality, the probe velocity in this direction is seriously limited. Second, in the conventional hopping mode it is common to set an excessive hopping height because the highest level for the scanning area of the sample is unknown. However, an excessive hopping height significantly increases the imaging time of the probe.

Herein we propose a new TFSM to improve upon the scanning speed of the traditional hopping mode without sacrificing its powerful detection capability. The core idea of TFSM is that it can set more reasonable hopping heights for each scanning line by quickly detecting the highest point of each scanning line of the sample, which greatly reduces the time consumption of imaging. Figures 1a-1e shows the process of imaging a sample with the TFSM, where Figure 1b illustrates the hopping height of each scanning line in the sample using the TFSM. It is obvious that TFSM is different from the conventional hopping mode. In the TFSM, the hopping heights depend on the highest point of each scanning line, while the constant hopping height set in the conventional hopping mode ignores the morphological characteristics of the sample.

The key to implementing TFSM is to control the probe so that it can quickly and reliably detect each highest point of the scanning line. This work presents a new method to rapidly obtain the highest points of each scanning line, as described below. Figures 1c-1e depict the detailed process of detecting the highest point of a scanning line in a sample with the TFSM, which is labeled as the m -line in Figure 1a. First, the probe moves toward the sample surface at a speed v_z along the z -direction, moving a distance Δz . Then, the sample is driven by an x -directional piezoelectric actuator to quickly move in the x -direction at a speed v_x . During this procedure, if the ionic current, i , of the SICM does not quickly decrease to a set value i_{set} , the probe will again move Δz in the z -direction and the sample will move in the x -direction at a speed $-v_x$. This procedure is performed repeatedly until i decreases to i_{set} , at which point the height value of line m is set at h_{max}^m (Fig. 1e). Based on the above-mentioned process, the SICM system has completed the detection of the highest point of the m -line.

Theoretical Comparison of the Conventional Hopping Mode and TFSM

To compare the scanning speeds of the conventional hopping mode and TFSM, we theoretically calculated the scans of the same area of a sample using the same micropipette with identical setting parameters for the two different modes. We separately calculated the scanning time for the m -line of the sample (Fig. 1a). First, we calculated the time consumption for scanning the m -line in the conventional hopping mode, T_m^{Hopping} , given as

$$T_m^{\text{Hopping}} = t_z^{\text{Hopping}} + t_x^{\text{Hopping}} = \sum_{n=1}^N \frac{h_0 - h_n^m}{v_z} + t_x^{\text{Hopping}}, \quad (1)$$

where t_z^{Hopping} and t_x^{Hopping} are the micropipette movement times in the z - and x -directions, respectively; v_z is the probe velocity in the z -direction; Δx the probe scanning step in the x -direction; h_0 the hopping height; and h_n^m ($n = 1, 2, \dots, N$) the height of the probe when the ion current reaches the set value for the n th pixel on the m -line. Next, we calculated the time required for scanning the m -line in the TFSM, T_m^{New} , given as

$$T_m^{\text{New}} = t_{\text{max}}^m + t_z^{\text{New}} + t_x^{\text{New}} = \frac{h_0 - h_{\text{max}}^m}{\Delta z} \times \frac{N \cdot \Delta x}{v_x} + \sum_{n=1}^N \frac{h_{\text{max}}^m - h_n^m}{v_z} + t_x^{\text{New}}, \quad (2)$$

where t_{max}^m is the time consumption for detecting the highest point of the m -line; t_z^{New} and t_x^{New} are the micropipette movement times in the z - and x -directions, respectively; Δz is the approach step distance in the z -direction during the detection of the highest point of the m -line; and h_{max}^m the height of the highest point of the m -line (i.e., the hopping height of the scanning line). Because the movement distance and the speed of the probe in the x -direction are the same in the two scanning modes, $t_x^{\text{New}} = t_x^{\text{Hopping}}$. To further compare the time used to scan the m -line of the sample in the TFSM and conventional hopping mode, we subtract equation (2) from equation (1) to obtain

$$\Delta T_m = N \times \left[(h_0 - h_{\text{max}}^m) \times \left(\frac{1}{v_z} - \frac{1}{\Delta z} \times \frac{\Delta x}{v_x} \right) \right]. \quad (3)$$

Equation (3) shows that a smaller h_{max}^m and a larger Δz reduce the time required in the TFSM compared with that of the conventional hopping mode. Novak et al. (2014) have measured the dynamic interaction between a nanoparticle and a living cell with v_z

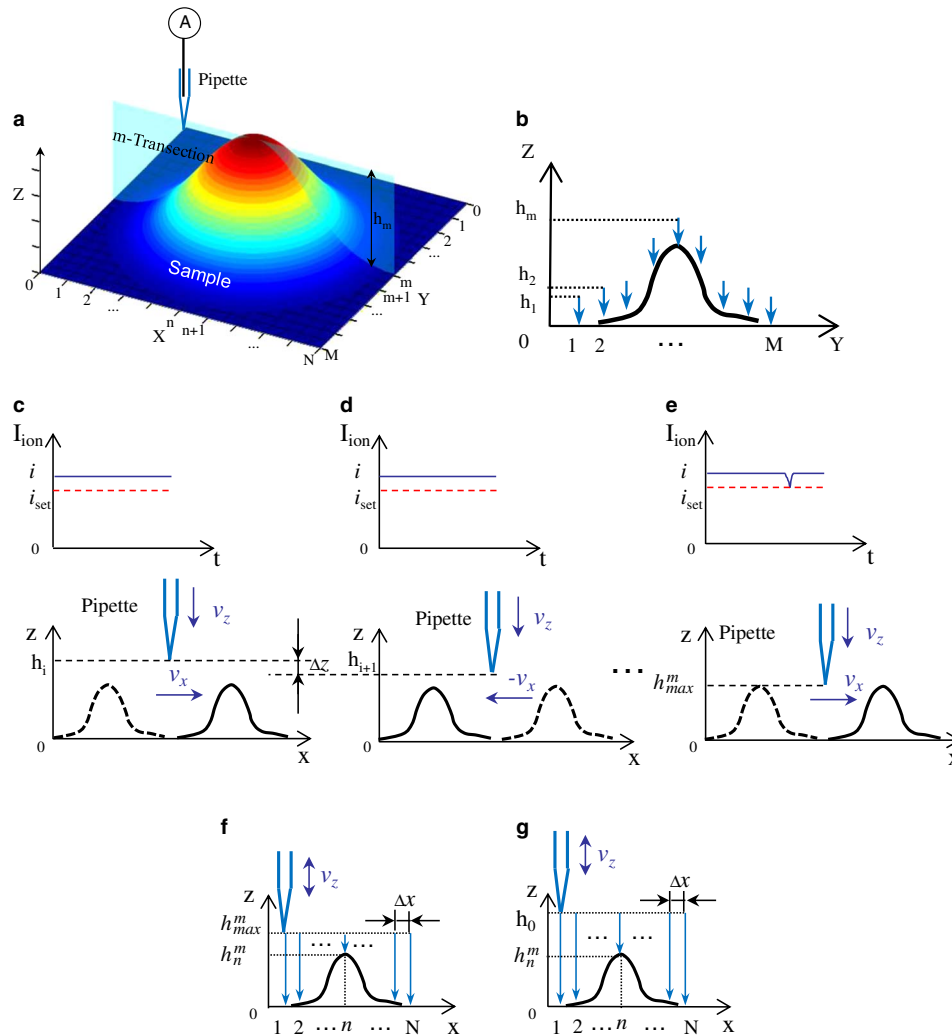


Figure 1. Schematic diagram of proposed scanning mode. **a:** The illustration of hopping height h_m corresponding to the m -transsection of the sample ($M \times N$, M and N is the numbers of rows and columns, respectively). **b:** The obtained hopping heights of the whole sample using horizontal fast scanning method. **c–e:** The process of detecting the highest point of m -line in horizontal fast scanning method. **f:** The scanning process of m -line in transverse fast scanning mode (TFSM) with automatically detecting the highest point. **g:** The scanning process of m -line in conventional hopping mode with the artificially setting hopping height.

up to 500 nm/ms by utilizing the double z -piezo structure that can rapidly withdraw the SICM probe. The single z -piezo is usually employed in the conventional hopping mode and the value of v_z is typically 50–200 nm/ms. In the literature, Jung et al. (2015) reported that the image artifacts began to appear on the surface of the sample as a result of the reduced stability when approach rate is 300 nm/ms. Watanabe & Ando (2017) have developed a high-speed XYZ-nanopositioner with vertical travel range of $\sim 6 \mu\text{m}$ and the tip approach rate is 400 nm/ms. To simplify the comparison of imaging time for the m -line of the sample, typical setting parameter values are input into equation (3). Next, we assume $v_z = 200 \text{ nm/ms}$, $v_x = 4 \text{ mm/s}$, $\Delta z = 100 \text{ nm}$, $\Delta x = 500 \text{ nm}$, $N = 100$, $h_0 = 5 \mu\text{m}$, and $h_{\text{max}}^m = 2.5 \mu\text{m}$. With these values we obtain a $\Delta T_m = 0.9375 \text{ s} > 0$, which clearly shows that the m -line imaging time of the TFMSM is less than that of the conventional hopping mode.

Theoretical Comparison of the Standing Approach (STA) Mode and TFMSM

Considering the STA mode (Takahashi et al., 2010) is another form of hopping mode in SICM, we compared the time

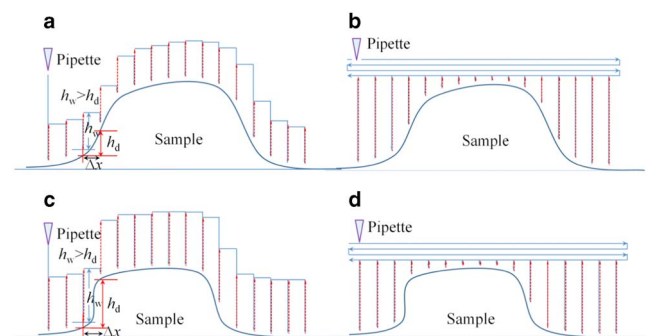


Figure 2. Comparison of standing approach (STA) mode and transverse fast scanning mode (TFMSM) for imaging the m -line of the sample. **a,c:** The scanning trajectories using STA mode for the flat and steep samples, respectively. **b,d:** The scanning trajectories using TFMSM for the flat and steep samples, respectively.

consumption of the STA mode and TFMSM for the m -line of the sample when other parameters are the same. As illustrated in Figures 2a and 2b, where Δx is the distance of the adjacent pixels, h_d the maximum height difference of the adjacent pixels, and

h_w the constant withdrawal amplitude in the STA mode. h_w should satisfy $h_w > h_d$ to realize STA mode in SICM, h_w should be minimized to obtain a higher imaging rate in the STA mode. For the steep samples, as illustrated in Figures 2c and 2d, even if the minimum h_w which satisfies $h_w > h_d$ is used in the STA mode, the imaging speed of the STA mode may be lower than that of the TFSM. Consequently, as a key parameter in the STA mode, h_w should be minimized and ensure the implementation of the STA mode. The STA mode has the advantage to image the flat samples. There is a withdrawal amplitude h_w which satisfies $h_d < h_w < h_c$ making the STA mode faster than TFSM, where h_c is called the critical amplitudes when the time consumptions of two modes is equal. Finally, The time consumption of the TFSM for a sample ($M \times N$), is given as:

$$T_{\text{total}}^{\text{New}} = \sum_{m=1}^M \left[\frac{h_0 - h_{\text{max}}^m}{\Delta x} \cdot \frac{N \cdot \Delta x}{v_x} + \sum_{n=1}^N \left(\frac{h_{\text{max}}^m - h_n^m}{v_z} \right) + t_x^{\text{New}} \right], \quad (4)$$

where $T_{\text{total}}^{\text{New}}$ is the total time consumption of the TFSM. The time consumption of the STA mode for the m -line of the sample is written as:

$$T_m^{\text{Stand}} = t_z^{\text{Stand}} + t_x^{\text{Stand}} = \frac{h_0 - h_1^m}{v_z} + \sum_{n=2}^N \frac{h^{mw} - (h_n^m - h_{n-1}^m)}{v_z} + t_x^{\text{Stand}}, \quad (5)$$

where t_z^{Stand} and t_x^{Stand} are the pipette movement times in the z - and x -directions, respectively; h^{mw} is the constant withdrawal amplitude of pipette. The time consumption for imaging a sample ($M \times N$) using STA mode is given as:

$$T_{\text{total}}^{\text{Stand}} = \sum_{m=1}^M \left[\frac{h_0 - h_1^m}{v_z} + \sum_{n=2}^N \frac{h^{mw} - (h_n^m - h_{n-1}^m)}{v_z} + t_x^{\text{Stand}} \right]. \quad (6)$$

We assume $T_{\text{total}}^{\text{Stand}} = T_{\text{total}}^{\text{New}}$, the critical withdrawal amplitude h^{mw} is calculated as follows:

$$h^{mw} = \frac{\sum_{m=1}^M \left(\frac{h_0 - h_{\text{max}}^m}{\Delta x} \cdot \frac{N \cdot \Delta x}{v_x} \right) + \sum_{m=1}^M \sum_{n=1}^N \left(\frac{h_{\text{max}}^m - h_n^m}{v_z} \right) - \sum_{m=1}^M \frac{h_0 - h_N^m}{v_z}}{\left(\frac{M \cdot (N-1)}{v_z} \right)}. \quad (7)$$

From equation (7), it can be seen that h^{mw} is determined by several scanning parameters and sample parameters. Based on

equation (7), we can estimate the value of h^{mw} and further compare the imaging speed of the STA mode and TFSM.

Parameter Settings of the TFSM Smart Hopping Mode

To realize the TFSM smart scanning mode, it is necessary to rapidly detect the highest point of each line of the scanned sample, with which can be set a more reasonable hopping height for each line. The value of the Δz approaching step directly influences the time for detecting the highest point, whereby a smaller Δz reduces the speed of detection but a larger Δz reduces the imaging stability. Using a scanning electron microscope (SEM) (SU8010, Hitachi, Tokyo, Japan), we measured the size of micropipette opening and investigated the approach curve of the micropipette to set a reasonable Δz (Fig. 3).

Theoretically, the probe detects the sample when the ion current begins to decrease. However, there are many kinds of experimental noise that lead to obtaining a false highest point. Therefore, we considered that the probe detected the highest point when the ion current decreased by 1% in actual experiments. As shown in Figure 3a, the distance between the tip of the micropipette and the sample surface was about 228 nm when the ion current decreased to the set point. In this paper, considering the detection speed and reliability, we set the approaching step Δz to 100 nm. Taking into account the influence of experimental environmental noise and the movement inertia of probe, the hopping height for each line was set as the sum of the height of the peak point of that line and the inner diameter of the micropipette opening, to improve the scanning speed without affecting the SICM imaging quality. As shown in the SEM image in Figure 3b, the probe opening radius is about 130 nm.

Instrumentation and Materials

Instrumentation

In the experiments, we used a home-built SICM system mainly composed of piezoelectric ceramic and a piezo-driver (Physik Instrument, Germany), Ag/AgCl electrodes, a nano-microprobe, 16-bit DA and AD modules, a patch clamp amplifier, core control chip (Xilinx FPGA), a host personal computer and a serial communication module.

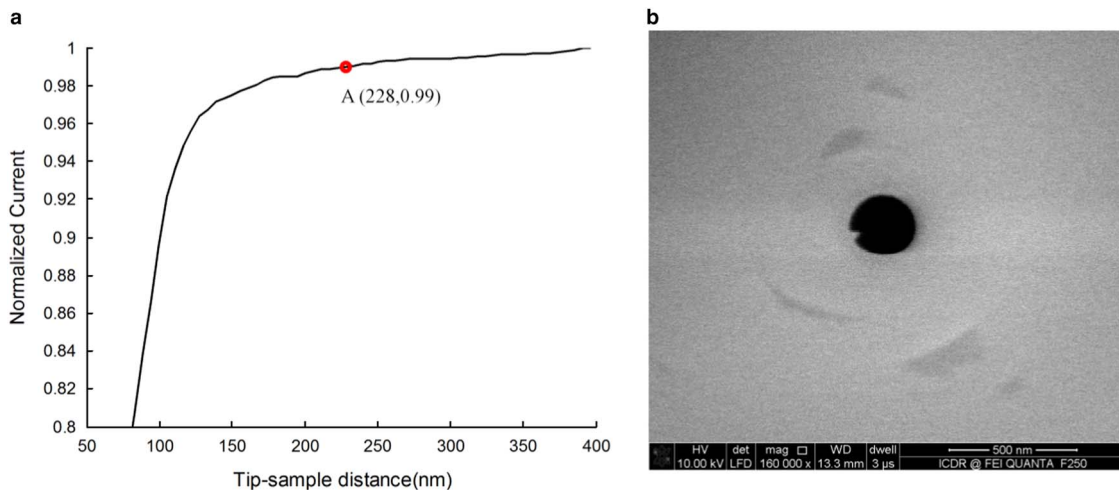


Figure 3. a: Approach curve of the micropipette. b: Scanning electron microscope image of the micropipette tip.

Pipettes

The SICM probes were selected from borosilicate capillaries (Sutter Instrument Company, Novato, CA, USA) with internal diameters of 0.58 mm, external diameters of 1 mm, and lengths of 10 cm. The borosilicate capillaries were pulled using a laser pipette puller (P-2000, Sutter Instrument Company), whereby different opening radii were obtained by adjusting the puller parameters. The opening radii of the probes were about 130 nm, which were used in sets of experiments.

Samples

A series of contrast experiments were carried out on PDMS samples and living cell samples. One PDMS sample featured cylinders (4 μm radius, 2.5 μm height) and the other PDMS sample exhibited six-pointed stars (20 μm circumscribed circle radius, 2.5 μm height). All the PDMS samples are fabricated using imprint lithographic methods. The living cell samples included cells from the human breast cancer cell lines MCF-7, MDA-MB-231, murine cardiomyocytes and hippocampal neuronal cell with complex morphology. The PDMS and living cell experiments, respectively, used a KCl (0.1 mol/L) solution and a cell buffer solution during scanning. The cell buffer solution was prepared by the following process: first, a certain mass of NaCl, Na_2HPO_4 , and NaH_2PO_4 were dissolved in ultrapure water, and the pH value of phosphate solution was then adjusted to 7.2 using an HCl (1 mol/L) solution. Finally, the buffer solution was filtered with filter paper (filtration pore 20 nm) and was sterilized.

Results and Discussion

Quantitative Evaluation Methods

To compare the imaging quality of the TFSM and the conventional hopping mode, a series of contrast experiments were carried out using the same micropipette and the same scanning speed in the same sample region. To highlight the performance of SICM in the TFSM, the TFSM and the conventional hopping mode measurements were repeated ten times on the PDMS and the living cells samples while holding the scanning parameters and the micropipettes constant and unchanged. The imaging quality and stability of the two scanning modes was then evaluated using the mean squared height fluctuation of the scanning images, given as (Zhuang et al., 2016)

$$\text{MSE} = \frac{\sum_{k=1}^L \left[\sum_{i=1}^M \sum_{j=1}^N (f_k(i, j) - \bar{f}(i, j))^2 \right]}{L \times M \times N}, \quad (8)$$

where $M \times N$ denotes the number of pixels in each image; L is the recorded total number of images in each scanning mode; $f_k(i, j)$ the height value of the pixel with coordinates (i, j) in the k th image; and $\bar{f}(i, j) = \sum_{k=1}^L f_k(i, j) / L$ is the mean value of $f_k(i, j)$ for L images.

To compare the imaging speeds of the TFSM and the traditional hopping mode, herein we used the average pixel imaging frequency to quantitatively represent the imaging speed. The specific calculation method is given as

$$f = L \times M \times N / \sum_{k=1}^L t_k \quad (9)$$

where f is the average pixel imaging frequency, t_k is the time consumption of scanning the k th image.

Comparison of Imaging Speed and Quality with Conventional Hopping Mode

The comparison experiments for the imaging speed were conducted by scanning PDMS samples of known height and scanning human breast cancer cell samples of unknown height. We scanned identical sample areas ten times using the same micropipette with the same scanning speed in the two different scanning modes in the self-built SICM system. The tip-sample distance during scanning greatly influenced the imaging quality (Thatenhorst et al., 2014; Rheinlaender & Schäffer, 2015), so we scanned the comparison experiment samples with a 1.0% set point (point "A" in Fig. 3a).

Sample 1 was a micro-cylinder array made of PDMS, where each micro-cylinder was 2.5 μm high and had a 4 μm radius. Sample 2 was a six-pointed star array made of PDMS, where each star was 2.5 μm high and had a 20 μm circumscribed circle radius. Figure 4 shows comparisons of the topography as measured with the TFSM (Figs. 4a, 4c) and the conventional hopping mode (Figs. 4b, 4d). The size of the images is 128 \times 128 pixels. Because the topographies of the PDMS samples were known before the measurements, the hopping height of the conventional hopping mode was set to 5 μm in the comparison experiments. In the TFSM, the Δz was set to 100 nm and the hopping height was set as the sum of the heights of the peak point of each scanning line and the inner diameter of the micropipette opening (~ 230 nm).

Figures 4e and 4f plot the average pixel imaging frequency and the mean squared error (MSE) of the height fluctuation, respectively, in the images obtained by the TFSM and the conventional hopping mode. The calculation results show that the average pixel imaging frequencies of the PDMS samples 1 and 2 are 21.46 and 23.19 Hz, respectively, in conventional hopping mode; while that in the TFSM are about 38.24 and 39.19 Hz, respectively (Fig. 4e). In TFSM, the pixel imaging frequencies of samples 1 and 2 are increased by 78.2 and 69.0%, respectively, from that of the conventional hopping mode. As shown in Figure 4f, the MSEs of imaging the PDMS samples 1 and 2 in the conventional hopping mode is 398.56 and 425.66 nm^2 , respectively; while that in the TFSM are 406.82 and 410.23 nm^2 , respectively.

Because of the unknown specific height of living cells, we set a large hopping height of 15 μm in conventional hopping mode, while the other scanning parameters were the same as used in the previous experiments. The experimental and analysis results are shown in Figure 5. The cell samples 1 (i.e., MDA-MB-231) and 2 (i.e., MFC-7) were scanned ten times in the same area (as shown in Figs. 5a, 5d) in the TFSM and conventional hopping mode. The results in Figure 5e show that average pixel imaging frequencies of cell samples 1 and 2 are 35.07 and 36.19 Hz, respectively, in TFSM; while that in the conventional hopping mode are 12.02 and 11.19 Hz, respectively. It is obvious that the pixel imaging frequencies of the cell samples 1 and 2 are increased by about 2.92 and 3.23 times in the TFSM, respectively, compared with that of the conventional hopping mode. As shown in Figure 5f, the MSEs of imaging the cell samples 1 and 2 in conventional hopping mode are 532.37 and 541.66 nm^2 , respectively; while that of the TFSM are 550.20 and 536.19 nm^2 , respectively.

The experimental results indicate that the average pixel imaging frequency of the TFSM is larger than that of the conventional hopping mode, and the MSEs in the two different scanning modes are approximately equal, whether imaging PDMS or living cells. Furthermore, the imaging speed for samples

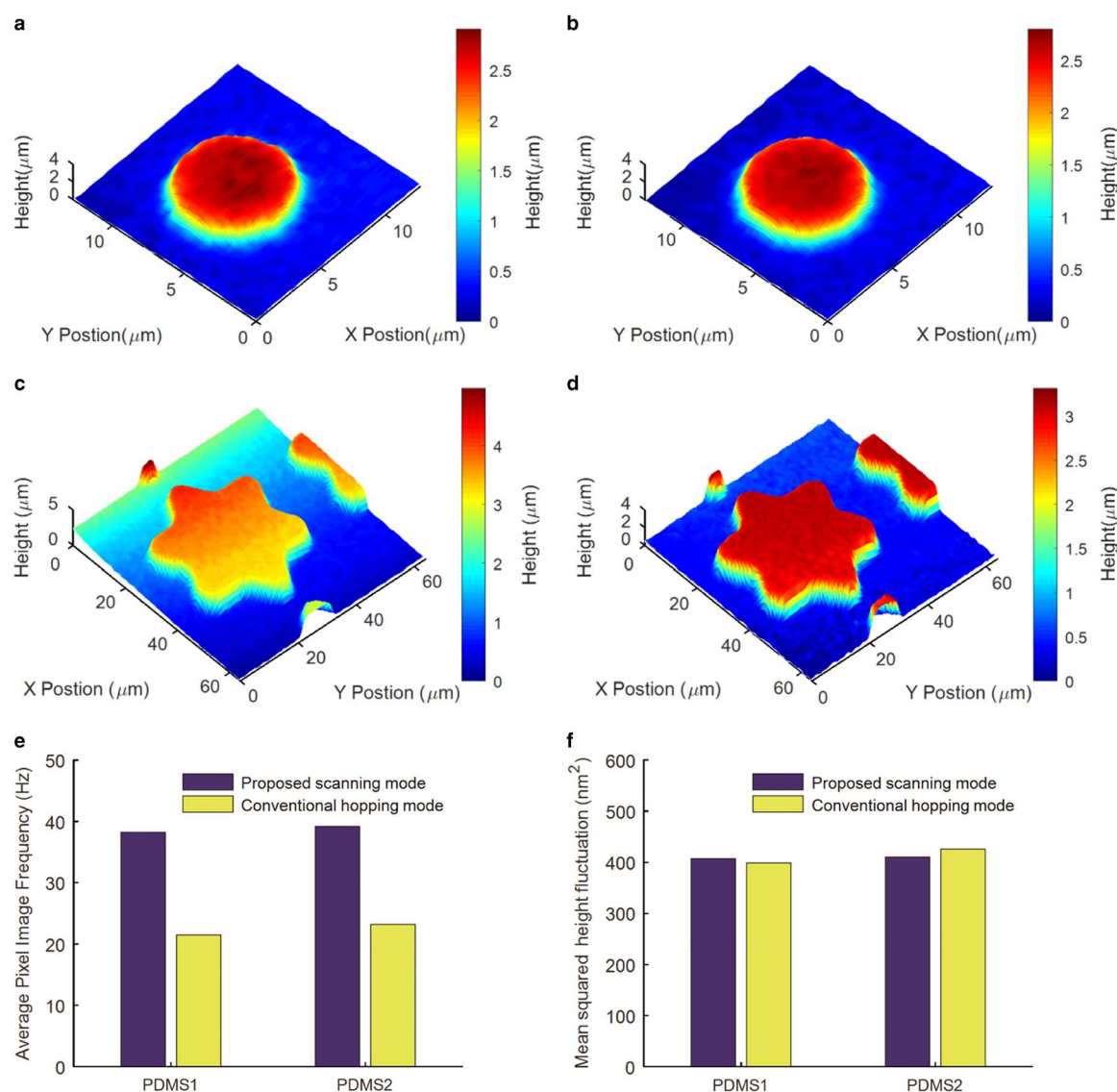


Figure 4. Comparison of imaging speeds and qualities for the polydimethylsiloxane (PDMS) samples with known height in transverse fast scanning mode (TFSM) and conventional hopping mode. **a:** Scanning image of PDMS 1 in TFSM. **b:** Scanning image of PDMS 1 in conventional hopping mode. **c:** Scanning image of PDMS 2 in TFSM. **d:** Scanning image of PDMS 2 in conventional hopping mode. **e:** Comparison of the average pixel imaging frequency for PDMS 1 and PDMS 2 in two scanning modes. **f:** Comparison of mean squared of scanning images height fluctuation of PDMS 1 and PDMS 2 in two scanning modes.

possessing unknown heights (i.e., living cell samples) is vastly improved over that of samples with known heights (i.e., PDMS samples).

The aim of this work is to optimize the scanning parameters and improve the imaging rate in the conventional hopping mode SICM. For imaging the samples with unknown topographies (such as cells, metals, and nonmetallic samples), the surface topographies of samples may be flat or extremely complex and even the locations are unknown. Therefore, the prescanning method (Zhukov et al., 2012) is usually adapted to obtain some knowledge of the sample morphology before the subsequent scan can be planned. Unfortunately, the prescanning method may not detect local abrupt sample structures and also reduce the scanning stability and imaging quality owing to the probe collision. Moreover, prescanning itself is also a very time-consuming task. Accordingly, to ensure scanning stability and imaging quality, a larger hopping height is usually employed in hopping mode SICM.

This paper not only focuses on the scanning of flat samples but also concerns the complex and unpredictable samples, such as neuron cells. In this section, the imaging speed of the conventional hopping mode (hopping height $15 \mu\text{m}$) and TFSM are compared using hippocampal neuron cells. The experimental and analysis results show that (Fig. 6) the average pixel imaging frequencies of the hippocampal neuron cell samples is increased by about 2.6 times in the TFSM, compared with that of the hopping mode (hopping mode: 11.23 Hz ; TFSM: 29.12 Hz), the MSEs of imaging the hippocampal neuron cell samples in two scanning mode is 356.82 and 338.56 nm^2 , respectively. The results further demonstrate the superiority of TFSM for complex cell samples. Next, we calculated the maximum slopes (dz/dx) of all samples in our SICM experiment and obtained the corresponding critical withdrawal amplitudes of the STA mode, which are shown in Table 1. It indicates there is a critical withdrawal amplitude which enables the imaging speed of the STA mode that is faster than that of TFSM. For example, the critical withdrawal

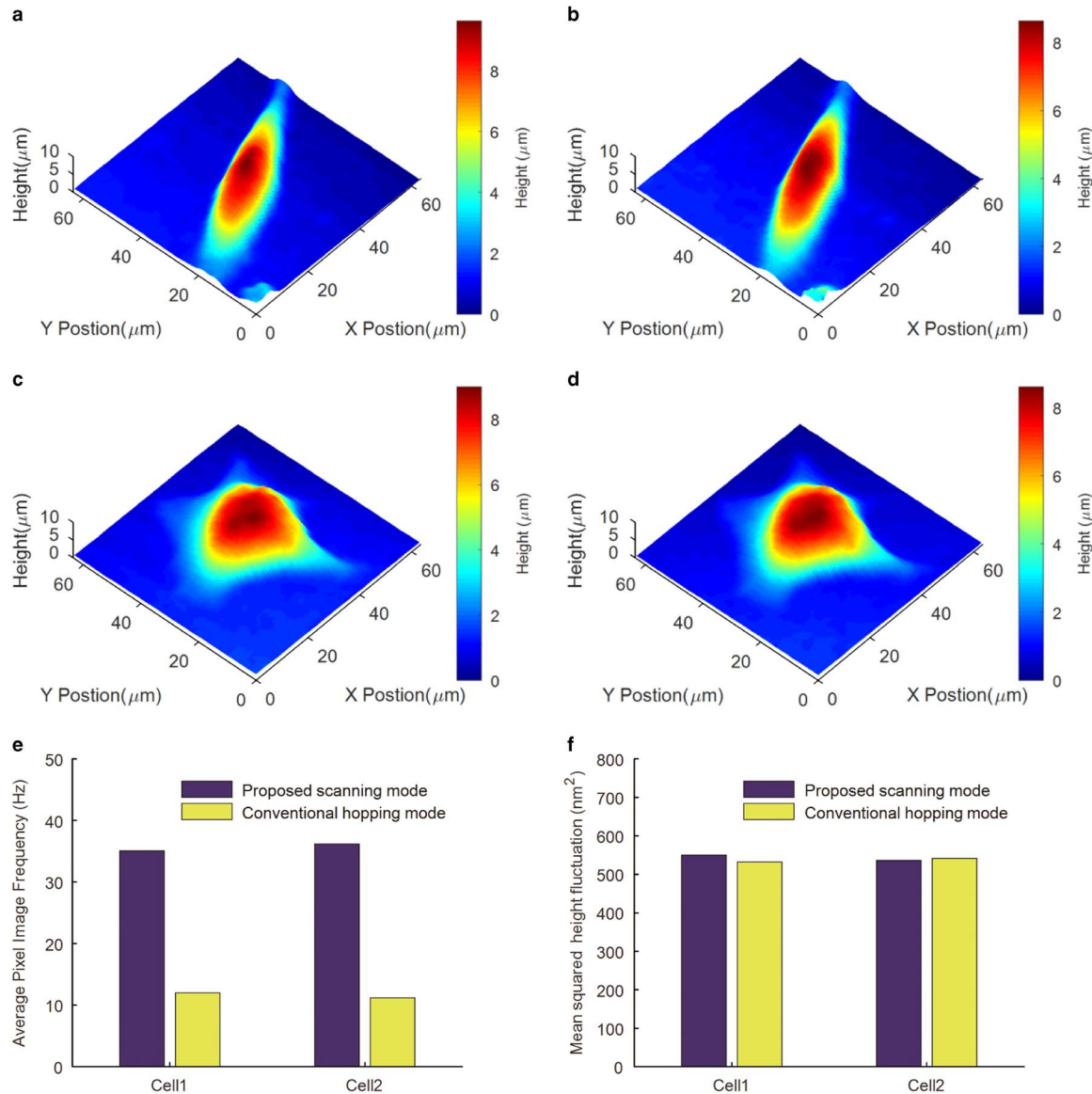


Figure 5. Comparison of imaging speeds and qualities for the human breast cancer cell samples with unknown height in transverse fast scanning mode (TFSM) and conventional hopping mode. **a,c:** The images of cell 1 (MDA-MB-231) and cell 2 (MFC-7) in TFSM, respectively. **b,d:** The images of cell 1 and cell 2 in conventional hopping mode, respectively. **e:** Comparison of average pixel imaging frequency for cell 1 and cell 2 in the two scanning modes. **f:** Comparison of mean squared of scanning images height fluctuation of cell 1 and cell 2 in two scanning modes.

amplitudes is $1.66\mu\text{m}$ when imaging the Cell2 (i.e., MFC-7) samples in the STA mode. In other words, the imaging speed of the STA mode is less than TFSM when h_w satisfies $0.43\mu\text{m} < h_w < 1.66\mu\text{m}$. It should be noted that the maximum slope of samples varies with the scanning direction. Although the STA mode has some advantage for imaging flat samples, it needs to predict the maximum slope of the samples for implementing a timesaving STA mode before conducting SICM scanning experiment. Moreover, the TFSM has more advantages for the larger slopes ($\sim 90^\circ$) samples.

Comparison of Imaging Speed (TFSM and Hopping Mode) with Different Hopping Heights

Here the aim is to further illustrate the advantages of TFSM considering the influences of the hopping heights. The comparison experiments were conducted by scanning the murine

cardiomyocytes (i.e., cell samples A) and MFC-7 (i.e., cell samples B) with different hopping heights (Figs. 7a-7f) in TFSM and conventional hopping mode, respectively. For the cell samples A and B, we set the hopping heights which decrease from 8 to $5\mu\text{m}$ and 20 to $15\mu\text{m}$ (Table 2), respectively. The calculated average pixel imaging frequencies of two methods are shown in Figures 7e and 7f. It can be seen from Figures 7e and 7f that whether the cell samples A ($100 \times 100\mu\text{m}^2$, 100×100 points) or B ($64 \times 64\mu\text{m}^2$, 128×128 points) are imaged with TFSM or conventional hopping mode, the average pixel imaging frequencies of the both methods increase with the decrease of the hopping heights. It can be also seen from Table 2 that when the hopping height of cell samples A and B are 8 and $20\mu\text{m}$, respectively, the average pixel imaging frequencies of the cell samples A and B are increased by 56 and 74% in TFSM, respectively, compared to that of the conventional hopping mode. The average pixel imaging frequencies of cell samples A and B are increased by 29.4 and 29.1%, when the

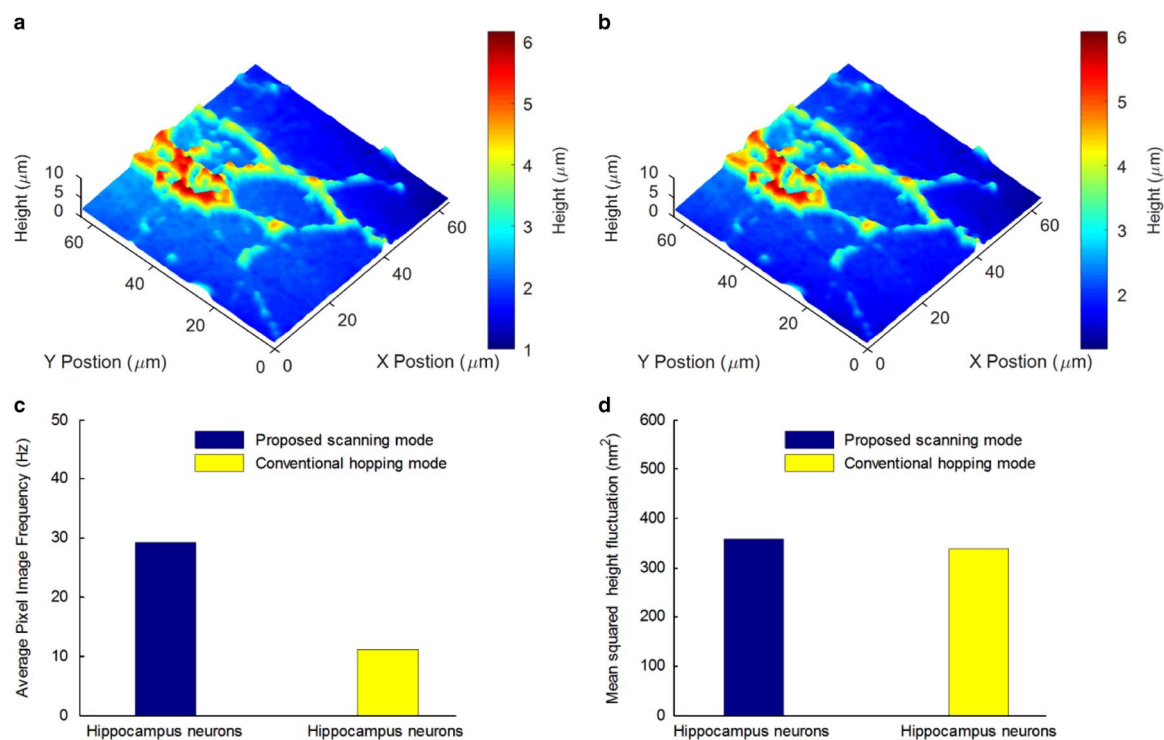


Figure 6. Comparison of imaging speeds and qualities for the hippocampal neuron cell samples with unknown height in transverse fast scanning mode (TFMS) and conventional hopping mode. **a:** Imaging result of hippocampal neuron cells in TFMS. **b:** Imaging result of hippocampal neuron cells in conventional hopping mode. **c:** Comparison of average pixel imaging frequency for hippocampal neuron cells in the two scanning modes. **d:** Comparison of mean squared of scanning images height fluctuation of hippocampal neuron cells in two scanning modes.

hopping heights are set to 5 and 15 μm, respectively, from that of the conventional hopping mode. Although the growth rates of average pixel imaging frequencies of TFMS compared with the conventional hopping mode decrease with the decrease of the hopping heights, they still increased by 29.4 and 29.1% when two dangerous hopping heights (cell samples A: 5 μm; B: 15 μm, respectively) are set.

Comparison of Imaging Speed and Stability with Previous Method (Zhuang et al., 2017)

In this part, considering the previous work (Zhuang et al., 2017) also used horizontal scanning to detect a change in the ion current to modify the hopping paths. First, we demonstrate the main differences of the two methods, and then compare their imaging speed and stability with PDMS samples and cell samples.

Table 1. Maximum Slopes of All Samples and the Corresponding Critical Amplitudes in Standing Approach (STA) Mode.

Samples	Maximum Slopes (dz/dx)	STA Mode [Critical Amplitudes (μm)]
PDMS1	71.34° (0.296/0.1)	~1.61
PDMS2	59.36° (0.843/0.5)	~1.52
Cell1 (MDA-MB-231)	48.24° (0.56/0.5)	~1.75
Cell2 (MFC-7)	40.70° (0.43/0.5)	~1.66
Hippocampal neuron cells	68.18° (1.249/0.5)	~4.65

In TFMS, the purpose of the horizontal scanning is that the pipette can quickly detect the highest point of each scanning line. In the previous method, the horizontal scanning is a predicted movement for upcoming raised topography in the next measurement point. TFMS mainly employs the tip detection capability in the vertical direction and the opening radius of the tip is the main parameter. While the previous work employs the tip detection capability in the sidewall direction and the half cone angle, the ratio of the inner to outer radius and the opening radii of the pipette tip are the main parameters.

The comparison experiments were conducted by scanning new PDMS and living cell samples (i.e., cell samples A and B). Both PDMS samples (i.e., PDMS A and B) featured cylinders. The pipette parameters in the experiments refer to the literature (Zhuang et al., 2017) and this study; all the other scanning parameters are the same. For the PDMS A (20 × 20 μm², 100 × 100 points), PDMS B (50 × 50 μm², 100 × 100 points), both the hopping heights were set to 5 μm. For the cell samples A (100 × 100 μm², 100 × 100 points) and B (64 × 64 μm², 128 × 128 points), the hopping heights were set to 5 and 18 μm. Moreover, 60 independent experiments were carried out for different measurement points (32 × 32, 100 × 100, and 256 × 256 points) using TFMS and the previous method. During the process of obtaining a single image, if the probe is fractured, the tip is blocked, the ion current feedback signal becomes abnormal, etc., in the scanning process, the scan is considered to have failed. Consequently, we define the success rate of scanning as $1 - N_{\text{failed}}/N_{\text{total}}$. Where N_{failed} denotes the number of failed images, N_{total} denotes the total number of scanning images. The statistical analysis for the success rate of scanning of two different methods was conducted. Figures 8e and 9e plot the average pixel imaging frequencies in the images obtained by TFMS and the previous

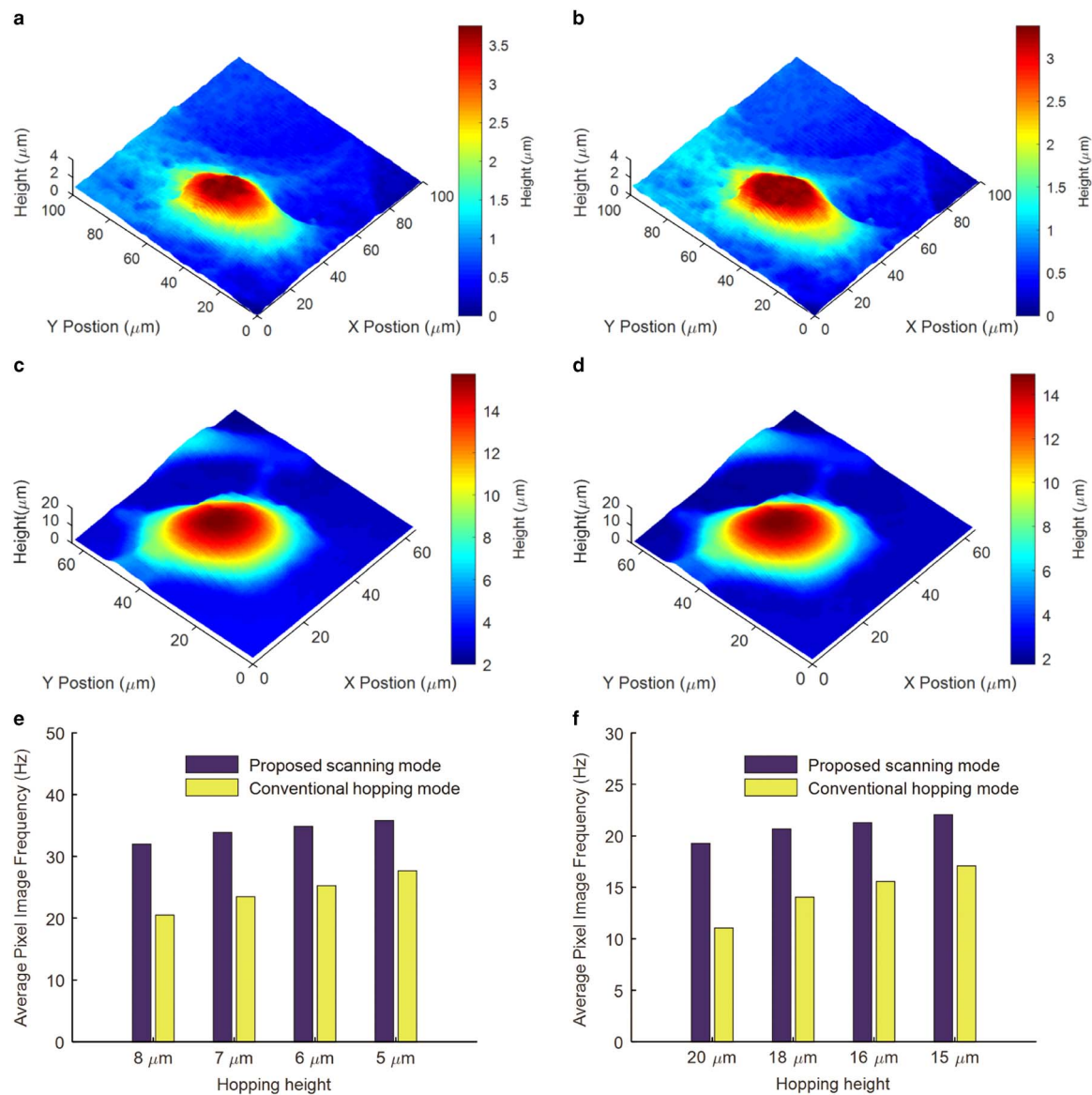


Figure 7. Comparison of imaging speeds for the cell samples A (murine cardiomyocytes) and B (MFC-7) with different hopping heights in transverse fast-scanning mode (TFSM) and conventional hopping mode. **a,c:** The images of cell A and B in TFSM, respectively. **b,d:** The images of cell A and B in conventional hopping mode, respectively. **e:** Comparison of average pixel imaging frequency for cell A with different hopping heights in two scanning modes. **f:** Comparison of average pixel imaging frequency for cell B with different hopping heights in two scanning modes.

method, respectively. The calculation results show that the average pixel imaging frequencies of the PDMS samples A and B are 36.29 and 35.88 Hz in TFSM; while that in the previous method are about 38.52 and 38.75 Hz. In addition, the average pixel imaging frequencies of cell samples A and B are 35.80 and 20.67 Hz in TFSM; while that in the previous method are 38.00

and 24.10 Hz. Figures 8f and 8g and Figures 9f and 9g plot the success rates of imaging in the two methods with different measurement points. The comparison results for the PDMS A, B, cell samples A and B in two methods are shown in Table 3.

As seen from the Table 3, the imaging speed of the previous method is larger than that of TFSM only when the

Table 2. Average Pixel Imaging Frequencies in Figures 7e and 7f.

Samples	Methods	Average Pixel Image Frequencies (Hz) [Hopping Height (μm)]			
Cell A	TFSM	32.015 (8 μm)	33.871 (7 μm)	34.856 (6 μm)	35.796 (5 μm)
	Hopping mode	20.501 (8 μm)	23.482 (7 μm)	25.265 (6 μm)	27.671 (5 μm)
Cell B	TFSM	19.269 (20 μm)	20.67 (18 μm)	21.278 (16 μm)	22.056 (15 μm)
	Hopping mode	11.053 (20 μm)	14.048 (18 μm)	15.565 (16 μm)	17.078 (15 μm)

TFSM, transverse fast-scanning mode.

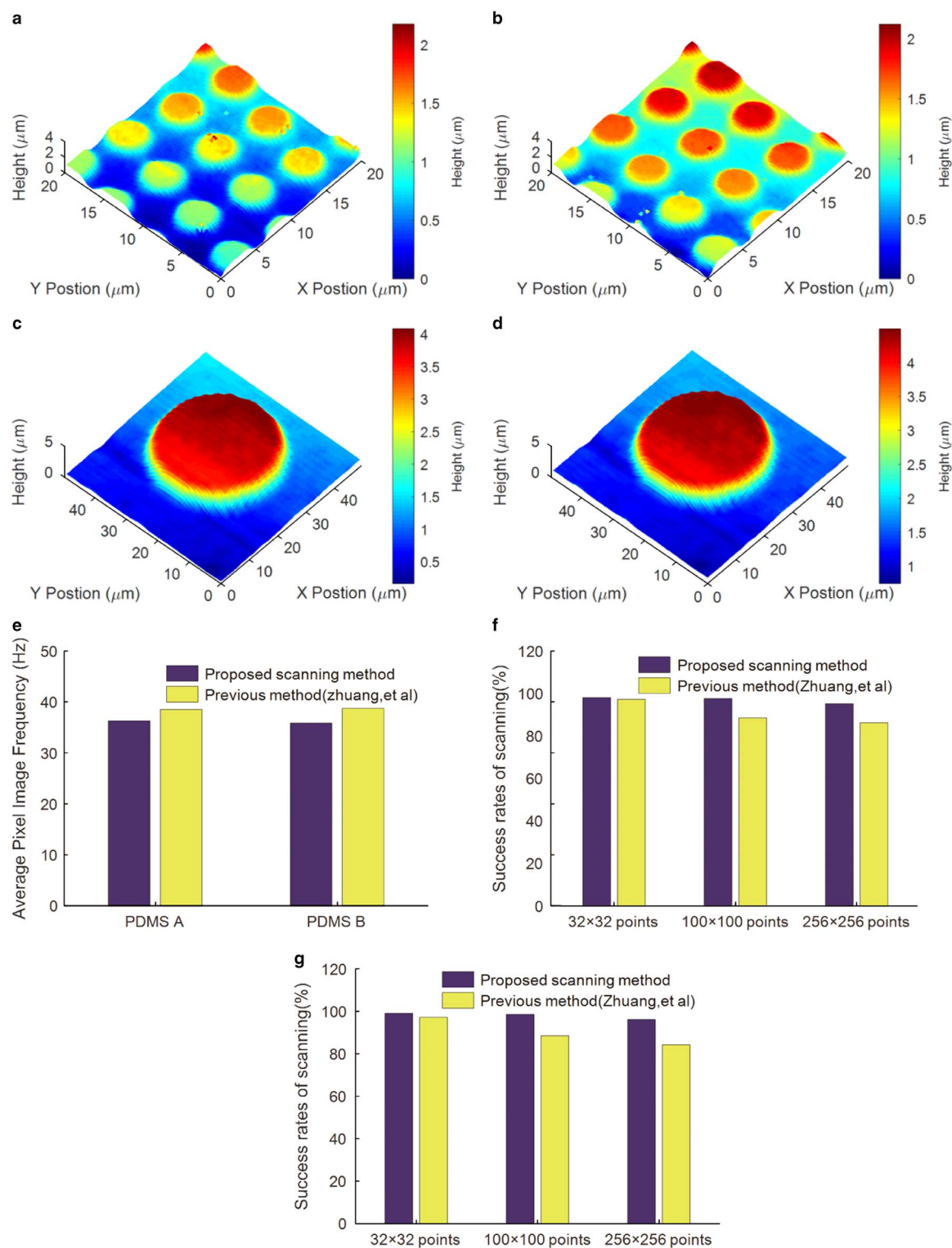


Figure 8. Comparison of imaging speeds and success rates of scanning for polydimethylsiloxane (PDMS) samples with different topographies in transverse fast-scanning mode (TFSM) and previous method. **a,c:** The images of PDMS A and PDMS B in TFSM, respectively. **b,d:** The images of PDMS A and PDMS B in previous method, respectively. **e:** Comparison of average pixel imaging frequency in two scanning methods. **f,g:** Comparison of success rates of scanning for PDMS A and PDMS B in two methods with different measurement points, respectively.

scanning process of the previous method has not failed. However, the success rate of the previous method is lower than that of TFSM whether scanning PDMS or living cell samples. This is mainly because there are more requirements for detecting the changes in ion current in the process of predicting

the upcoming raised topographies in the previous method, especially for the cell samples. The increasing interference factors that occur due to the physiological activities between cells in the cell environment affect the detecting process and finally lead to the decrease of predicting precision and the failure of scan.

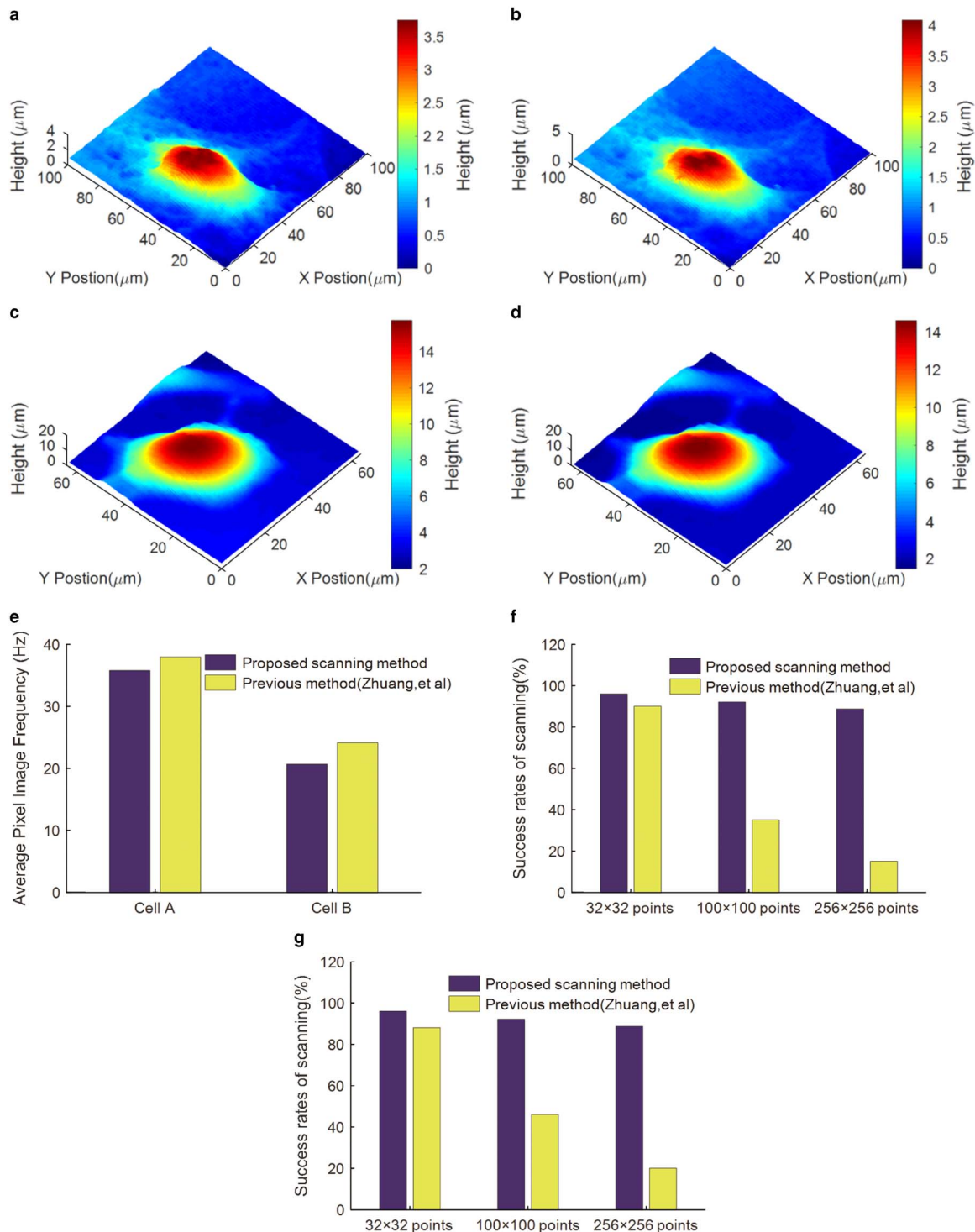


Figure 9. Comparison of imaging speeds and success rates of scanning for cell samples with different topographies in transverse fast-scanning mode (TFSM) and previous method. **a,c:** The images of cell A (murine cardiomyocytes) and cell B (MFC-7) in TFSM, respectively. **b,d:** The images of cell A and cell B in previous method, respectively. **e:** Comparison of average pixel imaging frequency in the two scanning methods. **f,g:** Comparison of success rates of scanning for cell A and cell B in two methods with different measurement points, respectively.

Influence of Scanning Direction on Imaging Speed of TFSM

To research the influence of the scanning direction on the imaging speed in TFSM, a series of experiments was conducted with cells from the MDA-MB-231 cell line. The same sample area was scanned from different directions using the same

micropipette with the same parameters. Herein, we define the initial scanning direction to be the 0° direction, and the scanning direction was subsequently changed by rotating the petri dish containing the cells. As shown in Figure 10, the images were obtained from the 0° , 45° , and 90° scanning directions, and the average pixel imaging frequency of the images obtained in TFSM

Table 3. Success Rates of Scanning with Different Number of Pixels.

Samples	Methods	Success Rates of Scanning (%) (Number of Pixels)		
		% (32 × 32)	% (100 × 100)	% (256 × 256)
PDMS A	TFSM (proposed method)	98.3	98.3	96.6
	Previous method (Zhuang et al., 2017)	95.0	91.6	86.6
PDMS B	TFSM	98.3	98.3	96.6
	Previous method	96.7	88.4	84.2
Cell A	TFSM	96.6	91.6	88.3
	Previous method	90.0	35.0	15.0
Cell B	TFSM	95	91.7	88.33
	Previous method	88.3	45	21.6

PDMS, polydimethylsiloxane; TFSM, transverse fast-scanning mode.

were found to be 66.9, 35.3, and 33.1 Hz, respectively. This result demonstrates that the average scanning speed varies with the scanning direction. From Principles of the Method section, we determined that the hopping height of the scanning depended on the highest point of each scanning line of the sample, so changing the scanning direction could lead to different hopping heights in the TFSM. In other words, there is an ideal scanning direction wherein the sum of the hopping heights and the scanning time consumption are both minimized. However, it is not only difficult, but also time-consuming to predict the sample shape before setting an ideal scanning direction. And for some samples, with approximately centrosymmetric shapes, it is no longer feasible to improve the imaging speed by changing the scanning direction.

Conclusions

This paper presents the TFSM of SICM to improve upon the imaging speed of the conventional hopping mode, where the feasibility and advantages of the TFSM are validated by both theoretical analysis and experimental studies. The TFSM can attain fast imaging by the setting of a reasonable hopping height for each scanning line that depends on the height of the highest point in each line. Using a home-built SICM system, a series of comparative experiments were carried out on PDMS samples with known feature heights, human breast cancer cells with unknown feature heights and hippocampal neuronal cells with complex topographies, using both the TFSM and conventional

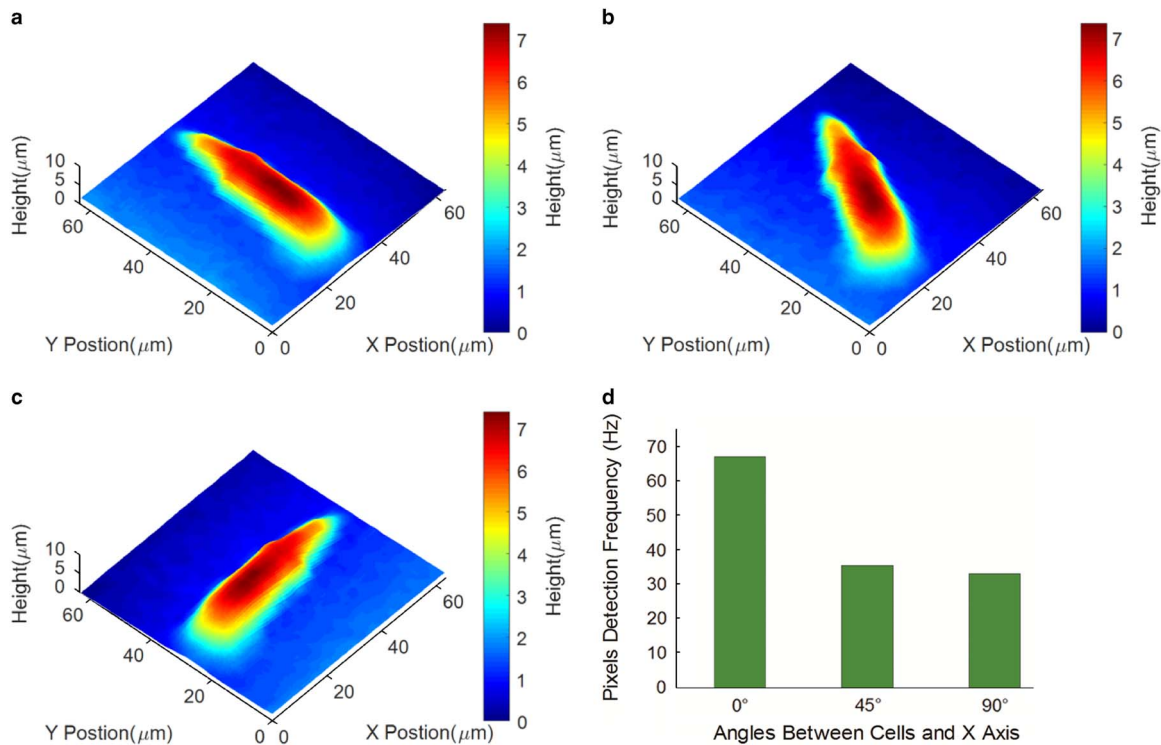


Figure 10. The influence of scanning direction on imaging speed in the transverse fast-scanning mode (TFSM). a: 0° direction; b) 45° direction; c) 90° direction; d) comparison of average pixel imaging frequency for cell 1 (MDA-MB-231) from different scanning directions using TFSM.

hopping mode. By comparing the imaging speed and imaging quality of the two different scanning modes, we show that the imaging speed of TFMS is greater, while the imaging quality of the two different modes are nearly identical. Moreover, further studies on the characteristics of the TFMS show that the imaging speed is related to the scanning direction of the probe.

In summary, herein we introduce a new scanning mode for fast SICM, and also create a new opportunity to realize fast imaging for samples with extremely complex morphologies.

Acknowledgments. The authors thank the National Natural Science Foundation of China (Project no. 51375363) and Industrial Research Project of Science and Technology Department of Shaanxi Province (Project no. 2013GY2-04) for funding this work. In addition, the authors are grateful for the permission to use the human breast cancer cell samples from the Bioinspired Engineering and Biomechanics Center at Xi'an Jiaotong University. The authors thank Dr. Wang Changhe from the School of Life Science and Technology in Xi'an Jiaotong University for providing the hippocampal neuron cell samples in this work.

References

- Babakinejad B, Jönsson P, López Córdoba A, Actis P, Novak P, Takahashi Y, Ferrer-Montiel A, Klennerman D and Korchev YE (2013) Local delivery of molecules from a nanopipette for quantitative receptor mapping on live cells. *Anal Chem* **85**(19), 9333–9342.
- Bruckbauer A, Ying L, Rothery AM, Zhou D, Shevchuk AI, Abell C, Korchev YE and Klennerman D (2002) Writing with DNA and protein using a nanopipet for controlled delivery. *J Am Chem Soc* **124**(30), 8810–8811.
- Hansma PK, Drake B, Marti O, Gould SAC and Prater CB (1989) The scanning ion-conductance microscope. *Science* **243**(4891), 641.
- Ivanov AP, Actis P, Jönsson P, Klennerman D, Korchev Y and Edel JB (2015) On-demand delivery of single DNA molecules using nanopipets. *ACS Nano* **9**(4), 3587–3595.
- Jung GE, Noh H, Shin YK, Kahng SJ, Baik KY, Kim HB, Cho NJ and Cho SJ (2015) Closed-loop ARS mode for scanning ion conductance microscopy with improved speed and stability for live cell imaging applications. *Nanoscale* **7**(25), 10989–10997.
- Korchev YE, Bashford CL, Milovanovic M, Vodyanoy I and Lab MJ (1997) Scanning ion conductance microscopy of living cells. *Biophys J* **73**(2), 653–658.
- Li P, Liu L, Wang Y, Yang Y, Zhang CLi G (2014) Phase modulation mode of scanning ion conductance microscopy. *Appl Phys Lett* **105**(5), 053113.
- Mann SA, Hoffmann G, Hengstenberg A, Schuhmann W and Dietzel ID (2002) Pulse-mode scanning ion conductance microscopy—A method to investigate cultured hippocampal cells. *J Neurosci Methods* **116**(2), 113–117.
- McKelvey K, Perry D, Byers JC, Colburn AW and Unwin PR (2014) Bias modulated scanning ion conductance microscopy. *Anal Chem* **86**(7), 3639–3646.
- Nadappuram BP, McKelvey K, Al Botros R, Colburn AW and Unwin PR (2013) Fabrication and characterization of dual function nanoscale pH-scanning ion conductance microscopy (SICM) probes for high resolution pH mapping. *Anal Chem* **85**(17), 8070–8074.
- Novak P, Li C, Shevchuk AI, Stepanyan R, Caldwell M, Hughes S, Smart TG, Gorelik J, Ostanin VP, Lab MJ, Moss GWJ, Frolenkov GI, Klennerman D and Korchev YE (2009) Nanoscale live-cell imaging using hopping probe ion conductance microscopy. *Nat Methods* **6**(4), 279–281.
- Novak P, Shevchuk A, Ruenaroengsak P, Miragoli M, Thorley AJ, Klennerman D, Lab MJ, Tetley TD, Gorelik J and Korchev YE (2014) Imaging single nanoparticle interactions with human lung cells using fast ion conductance microscopy. *Nano Lett* **14**(3), 1202–1207.
- O'Connell MA and Wain AJ (2014) Mapping electroactivity at individual catalytic nanostructures using high-resolution scanning electrochemical-scanning ion conductance microscopy. *Anal Chem* **86**(24), 12100–12107.
- Pastré D, Iwamoto H, Liu J, Szabo G and Shao Z (2001) Characterization of AC mode scanning ion-conductance microscopy. *Ultramicroscopy* **90**(1), 13–19.
- Proksch R, Lal R, Hansma PK, Morse D and Stucky G (1996) Imaging the internal and external pore structure of membranes in fluid: TappingMode scanning ion conductance microscopy. *Biophys J* **71**(4), 2155–2157.
- Rheinlaender J and Schäffer TE (2015) Lateral resolution and image formation in scanning ion conductance microscopy. *Anal Chem* **87**(14), 7117–7124.
- Şen M, Takahashi Y, Matsumae Y, Horiguchi Y, Kumatani A, Ino K, Shiku H and Matsue T (2015) Improving the electrochemical imaging sensitivity of scanning electrochemical microscopy-scanning ion conductance microscopy by using electrochemical Pt deposition. *Anal Chem* **87**(6), 3484–3489.
- Shevchuk AI, Frolenkov GI, Sánchez D, James PS, Freedman N, Lab MJ, Jones R, Klennerman D and Korchev YE (2006) Imaging proteins in membranes of living cells by high-resolution scanning ion conductance microscopy. *Angew Chem Int Ed Engl* **118**(14), 2270–2274.
- Shevchuk AI, Gorelik J, Harding SE, Lab MJ, Klennerman D and Korchev YE (2001) Simultaneous measurement of Ca^{2+} and cellular dynamics: combined scanning ion conductance and optical microscopy to study contracting cardiac myocytes. *Biophys J* **81**(3), 1759–1764.
- Takahashi Y, Murakami Y, Nagamine K, Shiku H, Aoyagi S, Yasukawa T, Kanzaki M and Matsue T (2010) Topographic imaging of convoluted surface of live cells by scanning ion conductance microscopy in a standing approach mode. *Phys Chem Chem Phys* **12**(34), 10012–10017.
- Takahashi Y, Shevchuk AI, Novak P, Murakami Y, Shiku H, Korchev YE and Matsue T (2010) Simultaneous noncontact topography and electrochemical imaging by SECM/SICM featuring ion current feedback regulation. *J Am Chem Soc* **132**(29), 10118–10126.
- Thatenhorst D, Rheinlaender J, Schäffer TE, Dietzel ID and Happel P (2014) Effect of sample slope on image formation in scanning ion conductance microscopy. *Anal Chem* **86**(19), 9838–9845.
- Watanabe S and Ando T (2017) High-speed XYZ-nanopositioner for scanning ion conductance microscopy. *Appl Phys Lett* **111**(11), 113106.
- Yang X, Liu X, Lu H, Zhang X, Ma L, Gao R and Zhang Y (2012) Real-time investigation of acute toxicity of ZnO nanoparticles on human lung epithelia with hopping probe ion conductance microscopy. *Chem Res Toxicol* **25**(2), 297–304.
- Zhuang J, Jiao Y and Mugabo V (2017) A new scanning mode to improve scanning ion conductance microscopy imaging rate with pipette predicted movement. *Micron* **101**, 177–185.
- Zhuang J, Li Z and Jiao Y (2016) Double micropipettes configuration method of scanning ion conductance microscopy. *Rev Sci Instrum* **87**(7), 073703.
- Zhukov A, Richards O, Ostanin V, Korchev Y and Klennerman D (2012) A hybrid scanning mode for fast scanning ion conductance microscopy (SICM) imaging. *Ultramicroscopy* **121**, 1–7.